NSRRC - J0492 U (2015)

RSC Advances

PAPER

View Article Online
View Journal | View Issue

Published on 13 October 2015. Downloaded by National Chiao Tung University on 13/11/2015 00:49:01.

CrossMark click for updates

Cite this: *RSC Adv.*, 2015, 5, 88500

Ternary morphology facilitated thick-film organic solar cell†

Jiangquan Mai,[a] Tsz-Ki Lau,[a] Ting Xiao,[b] Chun-Jen Su,[c] U-ser Jeng,[c] Ni Zhao,[b] Xudong Xiao[a] and Xinhui Lu*[a]

Received 26th August 2015
Accepted 11th October 2015

DOI: 10.1039/c5ra17268c

www.rsc.org/advances

Employing a thick active layer for organic photovoltaic (OPV) devices, holding great promise for enhanced light absorption and providing robust, pinhole-free films for large-scale fabrication, remains a great challenge. In this work, we propose a new route for fabricating thick-film OPV devices through a ternary bulk heterojunction system by combining a fullerene derivative with one high-crystallinity polymer and one high power conversion efficiency (PCE) polymer. As a demonstration, P3HT:PTB7:$PC_{71}BM$ ternary cells were fabricated, showing that they could maintain higher PCE with a thick active layer than both binary counterparts could. Synchrotron based grazing-incidence X-ray scattering results indicated that the ternary morphology gave rise to a smaller intermixing domain size and a favorable molecular orientation, which should be beneficial to charge separation and transport.

Introduction

Solution-processed organic photovoltaic (OPV) devices have attracted extensive attention due to their potential for offering low-cost, flexible, light-weight solar cells for clean energy harvesting. So far, most high efficiency OPV devices have been achieved with very thin active layers (<110 nm).[1,2] This thickness limitation is mainly attributed to the low exciton diffusion length which leads to a great amount of energy loss due to charge recombination and the inadequate charge transfer mobility for separated charges to transfer to the respective electrodes.[3] Only 60%–80% of incident photons were absorbed with this thickness. Therefore, one can foresee significant improvement of PV performance if thicker films can be employed. Furthermore, the capability of using thicker films would be valuable to providing robust, pinhole-free and stable performing devices for large-scale production.

However, employing thick active layer remains a grand challenge. For many years, P3HT was only polymer that was able to function with a thick active layer in PV devices. It could maintain its PCE at a thickness as high as ~1200 nm which was never reported for other polymers.[4] Recently, researchers gradually realized the importance of thick-film OPV and thereby several new high-performance thick-film polymers emerged. Peet *et al.* reported a bithiophene-*co*-thiazolothiazole copolymer which achieved a PCE of 4.6% at an optimal thickness of 170 nm.[5] Janssen *et al.* presented a new diketopyrrolopyrrole-based semiconducting polymer with high fill factor (FF) in a ~300 nm thick film.[6] Woo's group also reported a dialkoxylphenylene and benzothiadiazole-based polymer obtaining over 9% PCE with ~300 nm thick active layer.[7]

In this manuscript, we report a brand new route of fabricating high efficiency thick-film OPV devices. It is realized with a ternary organic polymer system, which employs prototype electron donor and acceptor materials poly(3-hexylthiophene-2,5-diyl) (P3HT) and [6,6]-phenyl-C_{71}-butyric acid methyl ester ($PC_{71}BM$) as the hosts and poly[4,8-bis[(2-ethylhexyl)oxy]benzo[1,2-*b*:4,5-*b*′]dithiophene-2,6-diyl-*alt*-3-fluoro-2-[(2-ethylhexyl)carbonyl]thieno[3,4-*b*]thiophene-4,6-diyl] (PTB7) as the sensitizer. Even though ternary OPV system has been extensively studied recently as an alternative route to tandem cells to broaden absorption spectrum by incorporating two light absorbing polymers with complementary absorption spectrum,[8–11] its potential of fabricating thick-film photovoltaic devices has never been explored before. Indeed, several ternary systems with cascade energy alignment[9,12,13] have shown reduced bimolecular recombination and increased mobility which are promising features for fabricating thick-film devices. Previous studies on P3HT:PTB7-Th:$PC_{71}BM$ merely focused on polymer photodetectors and broaden spectral response range from UV light to the near infrared region.[14] Here, we employed P3HT as the host polymer to utilize its remarkable ability of maintaining PCE in thick film, and the high performance polymer PTB7 as the sensitizer. We achieved a PCE of 4.6% with a ~200 nm film for ternary cell with P3HT : PTB7 : $PC_{71}BM$ mass ratio of 16 : 1 : 17.5, which significantly outperforms both

[a]Department of Physics, The Chinese University of Hong Kong, New Territories, Hong Kong. E-mail: xhlu@phy.cuhk.edu.hk

[b]Department of Electronic Engineering, The Chinese University of Hong Kong, New Territories, Hong Kong

[c]National Synchrotron Radiation Research Center, Hsinchu Science Park, 101 Hsin-Ann Road, Hsinchu, Taiwan

† Electronic supplementary information (ESI) available. See DOI: 10.1039/c5ra17268c

This journal is © The Royal Society of Chemistry 2015

Published on 13 October 2015. Downloaded by National Chiao Tung University on 13/11/2015 00:49:01.

P3HT:$PC_{71}BM$ and PTB7:$PC_{71}BM$ binary systems with similar active layer thickness. Grazing incidence wide angle and small angle X-ray scattering (GIWAXS/GISAXS) measurements were employed to investigate the ternary morphology.[15] The morphology results were correlated with the remaining of high PCE of ternary solar cells with increasing active layer thickness and demonstrated the feasibility of this new device optimization route, especially valuable for future large-scale manufacturing.

Experimental section

P3HT (Rieke Metals, 4002-E), $PC_{71}BM$ (American Dye Source ADS71BFA), PTB7 (LT-S9050 Lumtec) and PEDOT:PSS (VP Al 4083, H.C.Stack) were all used as received. P3HT, $PC_{71}BM$ and PTB7 were separately dissolved in *ortho*-dichlorobenzene (DCB) with 3% diiodooctane addictive as 40 mg ml^{-1}. After filtered through 0.45 μm PVDF syringe filter, the solution was mixed at different mass ratios. ITO substrates were cleaned stepwise with deionized water, acetone and isopropanol in ultrasonic cleaner for 10 min each and oxygen plasma treatment in the end. PEDOT:PSS was spun coated (4000 rpm, 60 s) on the cleaned ITO substrate and annealed under 130 °C for 20 min. The active layer was spun coated from ternary mixture solution on the top surface of PEDOT:PSS and dried in nitrogen atmosphere at room temperature for 3 hours. The thickness of active layer was controlled by tuning the spin speed. Next, 10 nm and 100 nm thick layers of Ca and Al were evaporated under vacuum at pressures of 1×10^{-5} Pa. Then samples were annealed on a hotplate at 150 °C for 10 min except for PTB7:$PC_{71}BM$ binary cells.

The solar cell performance was measured by a Keithley 2612 source meter unit under an AM 1.5G solar simulator with an intensity of 100 mW cm^{-2}. UV-vis absorption and photoluminescence spectrum were taken on a Cary 5G UV-vis-NIR spectrophotometer and a Hitachi F-4500 spectrofluorometer, respectively.

The GIXS measurements were conducted at 23A SWAXS beamline at the National Synchrotron Radiation Research Center, Hsinchu, Taiwan, using a 10 keV primary beam, 0.15° incident angle and Pilatus 1M-F and C9728DK area detector. GIXS samples were prepared on PEDOT:PSS coated silicon substrate by spin coating. The thickness of films was characterized by alpha step profilometer which has a system error of 20 nm.

Results and discussion

Device characteristics

Ternary P3HT:PTB7:$PC_{71}BM$ bulk heterojunction (BHJ) PV cells have been fabricated with different active layer thicknesses and optimized with various mass ratios. Fig. 1a and b show the corresponding current density *versus* voltage (*J–V*) characteristics under simulated AM 1.5G solar illumination at 100 mW cm^{-2} for the PV cells with a film thickness of ~100 and ~200 nm respectively. The mass ratio of P3HT : PTB7 : $PC_{71}BM$ ($a : b : c$) was kept to satisfy the relation $c = a + 1.5b$ in order to maintain the optimized mass ratios (1 : 1 and 1 : 1.5) for binary

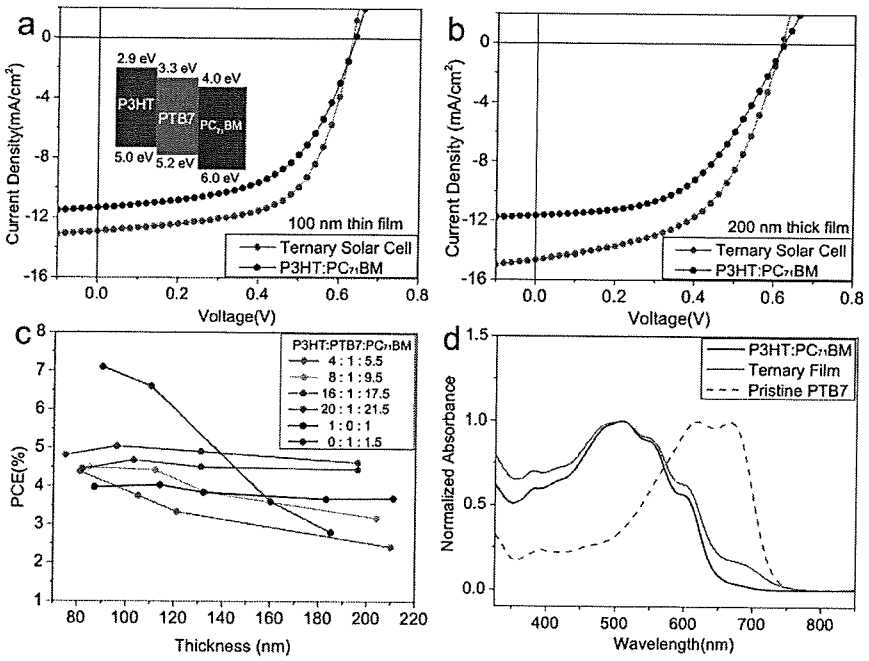

Fig. 1 (a) Representative *J–V* curves of ternary (P3HT : PTB7 : $PC_{71}BM$ = 16 : 1 : 17.5) and P3HT:$PC_{71}BM$ binary solar cells with ~100 nm active layer (inset: the energy level alignment diagram of P3HT : PTB7 : $PC_{71}BM$); (b) the corresponding *J–V* curves of devices with ~200 nm active layer; (c) the variation of PCEs with respect to active layer thickness for devices with different mass ratios; (d) UV-vis absorption spectra of pristine PTB7, binary P3HT:$PC_{71}BM$ and ternary films.

Published on 13 October 2015. Downloaded by National Chiao Tung University on 13/11/2015 00:49:01.

Table 1 Performance summary of binary solar cell and ternary solar cell[a]

Sample	V_{oc} (V)	J_{sc} (mA cm^{-2})	FF (%)	PCE (%)	Thickness (nm)	R_s (Ω)	R_{sh} (Ω)
P3HT : $PC_{71}BM$ (1 : 1) thin	0.64 ± 0.01	11.1 ± 0.6	56 ± 2	4.0 ± 0.1	114 ± 5	11.4 ± 0.5	502 ± 12
P3HT : PTB7 : $PC_{71}BM$ (16 : 1 : 17.5) thin	0.64 ± 0.01	12.9 ± 0.6	60 ± 1	5.0 ± 0.1	96 ± 3	6.6 ± 0.3	360 ± 9
P3HT : $PC_{71}BM$ (1 : 1) thick	0.63 ± 0.01	11.6 ± 0.2	51 ± 1	3.6 ± 0.1	211 ± 7	19.4 ± 0.7	704 ± 12
P3HT : PTB7 : $PC_{71}BM$ (16 : 1 : 17.5) thick	0.62 ± 0.01	14.6 ± 0.4	52 ± 1	4.6 ± 0.1	200 ± 6	10.3 ± 0.6	250 ± 10

[a] For thin films, the device characteristics are averaged over 5 devices. For thick films, they are averaged over 4 devices.

P3HT:$PC_{71}BM$ and PTB7:$PC_{71}BM$ cells simultaneously.[4,16] For comparison, the resultant device characteristics are summarized in Table 1. The cascade energy levels of P3HT, PTB7 and $PC_{71}BM$ are presented in inset of Fig. 1a. It suggests the band offsets between each component are large enough to provide sufficient driving force for photoinduced exciton to dissociate at P3HT/$PC_{71}BM$, PTB7/$PC_{71}BM$ and P3HT/PTB7 interfaces. This was confirmed by the steady state photoluminescence (PL) spectrum (ESI, Fig. S1†), since the PL of pristine P3HT and PTB7 was quenched significantly in the P3HT:PTB7 blend films suggesting efficient exciton dissociation at P3HT:PTB7 interfaces. The cascade energy alignment was reported to provide multiple carrier transfer paths to facilitate the charge transfer.[17–19]

At a film thickness of ~100 nm (Fig. 1a), the best performing ternary cell with a 16 : 1 ratio of P3HT : PTB7 achieved a PCE of 5.0%, with a short-circuit current density (J_{sc}) of 12.9 mA cm^{-2}, an open-circuit voltage (V_{oc}) of 0.64 V and a fill factor (FF) of 60%. The referencing P3HT:$PC_{71}BM$ binary cell with a similar film thickness gave a PCE of 4.0%, J_{sc} of 11.1 mA cm^{-2}, V_{oc} of 0.64 V and FF of 56%. Clearly, the overall 25% PCE improvement for the ternary cell is mainly due to the large enhancement in J_{sc} and FF. When the film thickness increases to ~200 nm (Fig. 1b), the binary P3HT:$PC_{71}BM$ cell gave a PCE of 3.6%. Remarkably, in this thickness, the ternary cell with a 16 : 1 ratio of P3HT : PTB7 also achieved a PCE of 4.6%, with a significant enhancement in J_{sc}. Interestingly, with the addition of PTB7, series resistance was reduced for both thicknesses, resulting in the increase of FF. This phenomenon was correlated with morphology results in the following section. Though the enhancement of FF is hindered by the low crystallinity of PTB7 in thick film, it can still maintain over 50% due to predominance of P3HT. On the contrary, as shown in Fig. 1c, when it comes to a thickness of 200 nm, the binary PTB7:$PC_{71}BM$ cell suffers a dramatic PCE degradation from 7.1% to 2.8% with a large drop in J_{sc} and FF. The performance degradation with a thick film was mainly attributed to the relatively low polymer domain crystallinity of PTB7 which is not able to provide efficient charge transport within the thick film. Fig. 1c presents the PCE of ternary PV cells with different mass ratios as a function of film thickness, where the thickness is varied by controlling the spin speed in spin coating process. Higher concentration of PTB7 in ternary cells resulted in more rapid PCE decrease with increasing thickness. This could be reasonably attributed to the relatively low polymer domain crystallinity of PTB7 as well. When the mass ratio of PTB7 : P3HT is equal to or less than 1 : 16, P3HT become the predominant component and begin to support the film to maintain its PCE, when the active layer thickness increases. As it is shown in Fig. 1c, ternary solar cells (16 : 1 : 17.5) have similar performance deterioration behavior (~10% drop) with binary P3HT:$PC_{71}BM$ solar cells but still remarkably outperform the binary film at 200 nm thick film. To investigate the changes in absorption with the addition of PTB7, UV-vis absorption spectra of P3HT:$PC_{71}BM$ blend film, ternary film (P3HT : PTB7 : $PC_{71}BM$ = 16 : 1 : 17.5) and pristine PTB7 film were measured, as shown in Fig. 1d. The absorption profile of the ternary film was similar to P3HT:$PC_{71}BM$ blend film with the maximum located at ~510 nm, indicating P3HT phase was still the main light absorber in the present ternary films. The presence of a shoulder at ~600 nm indicates to the unperturbed π–π stacking of P3HT in the ternary film. The absorption contribution of PTB7 was reflected by the appearance of a shoulder from 650 nm to 700 nm, which agreed with the absorption maximum of PTB7 at 670 nm.[2] The external quantum efficiency (EQE) spectra of the ternary and binary devices were also measured (Fig. S2†). Besides a slight increase in the range from 650 nm to 700 nm due to the PTB7 absorption, the EQE values are most enhanced in the region between 400 nm and 600 nm where P3HT:$PC_{71}BM$ show strong absorptions. This suggests that the extended absorption range by adding a small amount of PTB7 could not be the main reason of the observed J_{sc} improvements in ternary cells. Other reasons, most likely morphological changes, are to be explored.

Morphology characterizations of ternary films

The active layer morphology has known to be crucial to the device performance and was extensively investigated in binary systems.[20–22] However, studies on the morphology of ternary system are still very limited.[23] Grazing incidence X-ray scattering has proven to be one of the most efficient and non-destructive ways to obtain the bulk morphology and structural information of the active layer.[24–26] Specifically, GIWAXS provides detailed molecular level structural information of the active layer, such as lamellar spacing, π–π stacking spacing, crystallinity and molecular packing orientation,[24,26,27] while GISAXS reveals the phase separation information of the film.[28–30]

Fig. 2a and b present the GIWAXS patterns of binary P3HT : $PC_{71}BM$ films and the ternary film with the best performing mass ratio (16 : 1 : 17.5). The GIWAXS pattern of P3HT:$PC_{71}BM$ binary film (Fig. 2a) exhibits a scattering peak at

 This journal is © The Royal Society of Chemistry 2015

Published on 13 October 2015. Downloaded by National Chiao Tung University on 13/11/2015 00:49:01.

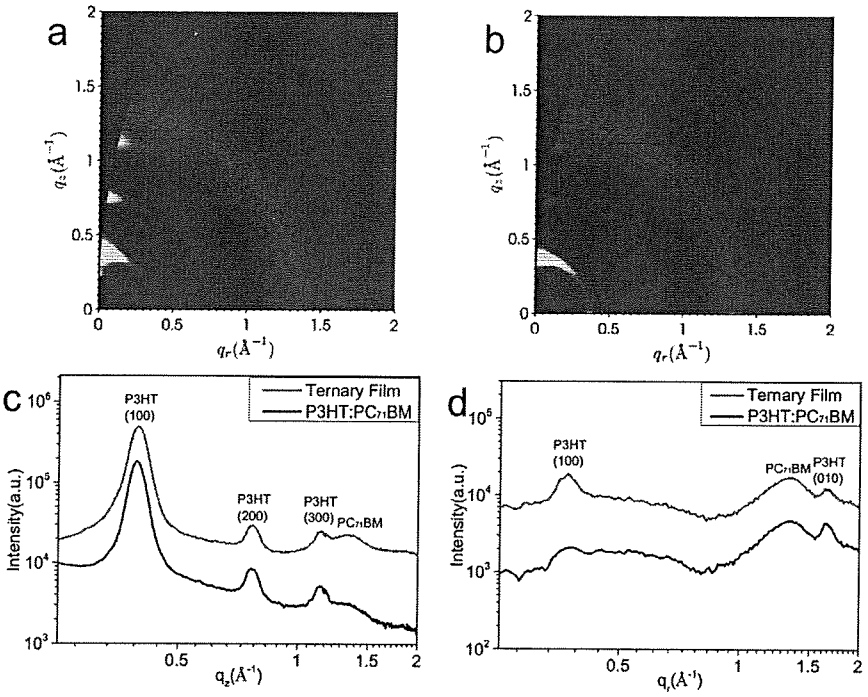

Fig. 2 GIWAXS patterns of (a) P3HT : $PC_{71}BM$ (1 : 1) binary film, (b) P3HT : PTB7 : $PC_{71}BM$ (16 : 1 : 17.5) ternary film; the intensity integration along (c) q_z axis and (d) q_r axis, respectively (displaced for clarity).

$q \approx 0.39$ Å^{-1} along the q_z axis, corresponding to the lamellar stacking of P3HT domains along the surface normal direction with a layer stacking of ~16 Å. The corresponding π–π stacking peak locates at $q \approx 1.65$ Å^{-1} (3.8 Å layer spacing) along the q_r axis. This is consistent with previous reports that the P3HT domains are "edge-on" oriented in P3HT:PCBM films.[31,32] In the GIWAXS pattern of the ternary film (P3HT : $PC_{71}BM$: PTB7 = 16 : 1 : 17.5) (see Fig. 2b), we can clearly identify the P3HT lamellar (100) peak along the q_z axis and the π–π peak along the q_r axis, suggesting P3HT domains are still predominantly edge-on oriented in the ternary films. However, the lamellar peak spans a larger polar angle (~9°) than in the P3HT:$PC_{71}BM$ binary film (~5°), suggesting a reduced edge-on order induced by the incorporation of the ternary PTB7 phase (Fig. S5†).

Detailed scattering profiles along q_z and q_r axis provide quantitative structural information about the semicrystallites within the film in the direction normal ("out-of-plane") or parallel ("in-plane") to the film surface, as plotted in Fig. 2c and d respectively. The scattering peaks were fitted well by Gaussian model. The lattice constants of the polymer semicrystallites can be calculated by 2π over the fitted Gaussian peak center ($2\pi/q_0$) and the average grain size or coherence length can be estimated by π over the standard deviation (π/σ) based on Scherrer equation.[33] The calculation result of P3HT crystallites coherence lengths D_{100} are listed in Table 2. Fig. 2c shows the scattering profiles along q_z by integrating the two-dimensional (2D) scattering pattern around q_z axis, corresponding to the out-of-plane structure. For both P3HT:$PC_{71}BM$ binary film and ternary film, where P3HT were the dominant polymer phase, lamellar peaks of P3HT were observed up to third order (0.39 Å^{-1}, 0.77 Å^{-1}, 1.14 Å^{-1}), demonstrating strong edge-on order. The calculated coherence length of edge-on domains in ternary film is ~14 nm a little smaller than that in P3HT:$PC_{71}BM$ binary film which is ~15 nm. This suggests the edge-on order of P3HT domains was slightly disturbed by the addition of PTB7 phase. Nevertheless, no PTB7 scattering signal can be identified in the scattering profile of the ternary film, due to the tiny population of PTB7 compared to the other two phases. In Fig. 2d, we plotted the scattering profiles *versus* q_r axis in order to study the in-plane structure. We observed that the scattering peak at $q_r = 1.65$ Å^{-1}, corresponding to π–π stacking of edge-on oriented P3HT domains, became weaker in agreement with our conclusion of the decrease of edge-on order. On the other hand, the scattering peak ($q = 0.38$ Å^{-1}) corresponding to the lamellar stacking in face-on oriented P3HT domains became stronger. It suggested that despite the slight decrease of edge-on order, the addition of a small amount of PTB7 facilitated the formation of face-on oriented P3HT domains, which are known to have high vertical mobility and be favorable for charge transport in OPV devices.[34,35] This could contribute to better device performance in ternary devices.

To understand the phase separation and to establish an overall picture of the nanoscale morphology in the bulk ternary films, GISAXS patterns were measured simultaneously with GIWAXS patterns. Since the concentration of PTB7 is so low in the optimized ternary solar cell that GISAXS signal mainly come from the structures of P3HT and $PC_{71}BM$, for fair comparison PTB7:$PC_{71}BM$ binary cell is not included as a control. Fig. 3a

Published on 13 October 2015. Downloaded by National Chiao Tung University on 13/11/2015 00:49:01.

Table 2 Structure parameters fitted from the GISAXS and GIWAXS profiles

Film	φ [%]	R [nm]	P	ξ [nm]	S_v [$\times 10^{-3}$ Å^{-1}]	$S_v/[\varphi/R]$	D_{100} [nm]
P3HT : $PC_{71}BM$ (1 : 1)	9.02	8.10	0.188	37.4	4.48	4.03	15
P3HT : PTB7 : $PC_{71}BM$ (16 : 1 : 17.5)	7.12	8.11	0.199	17.4	3.94	4.52	14

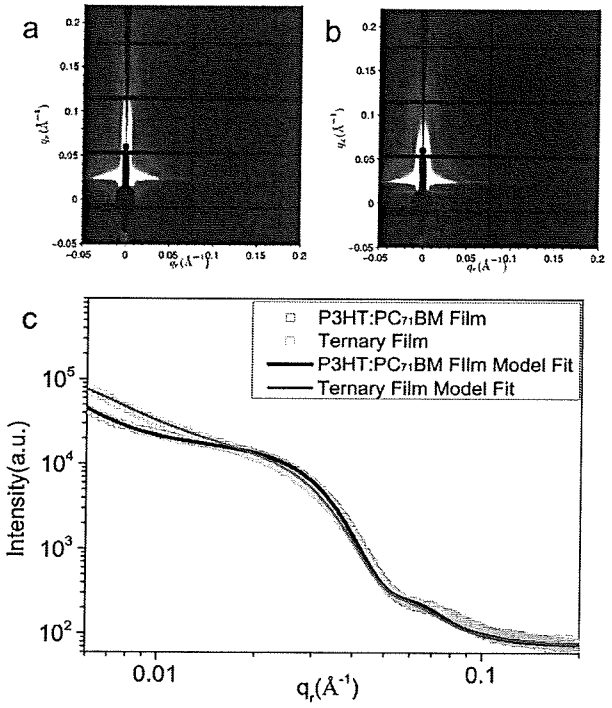

Fig. 3 GISAXS patterns of (a) P3HT : $PC_{71}BM$ (1 : 1) binary film and (b) P3HT : PTB7 : $PC_{71}BM$ (16 : 1 : 17.5) ternary film. (c) GISAXS profiles along q_r axis for (black squares) P3HT:$PC_{71}BM$ and (red squares) P3HT:PTB7:$PC_{71}BM$. The solid curves are best fittings with fitting parameters summarized in Table 2.

and b present the GISAXS patterns for binary P3HT : $PC_{71}BM$ (1 : 1) and ternary P3HT : $PC_{71}BM$: PTB7 (16 : 1 : 17.5) films. In both patterns, the appearances of a vertical streak at $q_r = 0$ and a horizontal streak at $q_z \approx 0.025$ Å^{-1} are signatures of GISAXS measurements due to diffuse reflectivity and "Yoneda" enhancement at the critical angle of the sample, respectively.[36] The scattering intensity profiles along q_r axis were extracted at reflected beam position ($q_z = 0.027$ Å^{-1}) for an enhanced signal. Fig. 3c demonstrates the obtained intensity profiles for binary P3HT : $PC_{71}BM$ (1 : 1) and ternary P3HT : PTB7 : $PC_{71}BM$ (16 : 1 : 17.5) films. In general, the two profiles resembled each other with the major difference appeared at low q region ($q <$ 0.03 Å^{-1}), indicating a morphology change at relatively large length scale.

Quantitative phase separation information could be obtained by fitting the GISAXS profiles with proper models.[28,29,37–39] Since GISAXS is simply measuring the scattering contrasts of different phases in the sample, a proper model should be able to capture the scattering contribution of all the phases with sufficient scattering contrast. For binary polymer:fullerene systems, several models were proposed and successfully explained the phase separation behaviors upon various fabrication conditions. Aggregated fullerene clusters were usually modeled as polydispersed hard spheres.[38,40] Polymer semicrystallites were also modeled as polydispersed hard spheres[29] or ignored[39,40] depending on their population and scattering contrast with the surrounding environment. The intermixing amorphous polymer and fullerene region were modeled as randomly distributed two phases[28,38,41] or fractal networks.[29] Here, for our ternary case, the scattering contribution from PTB7 could be ignored due to its small contribution. Consequently, the system could be simplified to a binary P3HT:$PC_{71}BM$ system. We adopted the model proposed by H.-C. Liao *et al.*,[38] which assumes the total scattering intensity is mainly from two terms: (1) $PC_{71}BM$ dispersed P3HT-rich domains and (2) $PC_{71}BM$ clusters. The formula for the scattering intensity is written as eqn (1)

$$I(q) = \frac{A_1}{\left[1 + (q\xi)^2\right]^2} + A_2\langle P(q,R,z)\rangle S(q,R,\varphi) + B \qquad (1)$$

where q is the scattering wave vector, A_1 is independent fitting parameter, A_2 is a function of $PC_{71}BM$ cluster volume fraction φ and scattering contrast $\Delta\rho$, and B is the background. The first term is the Debye–Anderson–Brumberger (DAB) model which models the $PC_{71}BM$ dispersed P3HT-rich region as randomly distributed phases with averaged correlation length of ξ. The second term corresponds to the contribution from $PC_{71}BM$ clusters modeled as polydispersed hard spheres. Here, $\langle P(q,R,z)\rangle$ is the form factor of spheres with average radius R following Schultz size distribution.[42,43] $S(q,R,\varphi)$ is the structure factor of hard spheres under Percus–Yevick approximation.[44] Herein, by fitting the intensity profiles with eqn (1), we could obtain the fitting parameters: average radius R, volume fraction φ and polydispersity $P\,(P = (1+z)^{-\frac{1}{2}})$ of $PC_{71}BM$ clusters and the correlation length ξ of the $PC_{71}BM$ dispersed P3HT-rich region. The total interface area per unit volume S_v, was also calculated based on Porod approximation.[38,45] The ratio of S_v to φ/R should be a constant if $PC_{71}BM$ clusters are isolated and decrease if the clusters are attached or aggregating. All the fitting parameters are summarized in Table 2.

Combining the fitting results of GIWAXS and GISAXS, we could first roughly compare the average sizes of three dominant phases: P3HT semicrystallites (D_{100}), $PC_{71}BM$ cluster ($2R$) and intermixing domain (ξ) for binary and ternary thin films. Clearly, the size of P3HT semicrystallites (~14 nm) and $PC_{71}BM$ clusters (~16 nm) remained almost the same with the addition

 This journal is © The Royal Society of Chemistry 2015

Published on 13 October 2015. Downloaded by National Chiao Tung University on 13/11/2015 00:49:01.

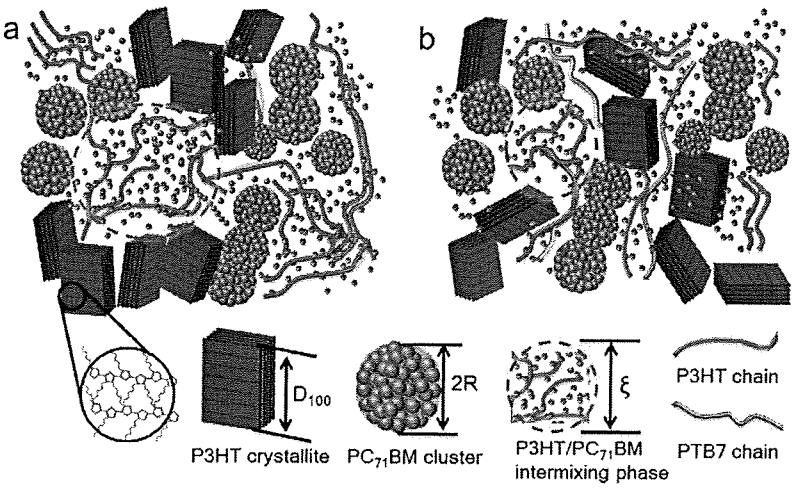

Fig. 4 Schematics of nanoscale morphologies for (a) binary and (b) ternary films. The blue spheres represent $PC_{71}BM$ molecules; the red blocks represent the P3HT crystals; the P3HT/$PC_{71}BM$ intermixing phases are highlighted with red and yellow dashed circles; the red chains and green chains represent the P3HT and PTB7 polymers respectively.

of a small amount of PTB7, being comparable to the predicted exciton diffusion length,[46] which will allow efficient exciton dissociation generated in these domains. However, the population of both phases decreased a little, as indicated by the slight decrease of P3HT lamellar peak intensity in GIWAXS and the decrease of fitted volume fraction of $PC_{71}BM$ clusters in GISAXS. Thus, the scattering results indicated a little growth of the overall population of intermixing region. This seems to contradict with the fitting results of the correlation length ξ of the intermixing domains, which decreased from 37.4 nm to 17.4 nm. Indeed, this provided us insights about the spatial distribution of the P3HT semicrystallites or $PC_{71}BM$ clusters. Based on the similar ratio of S_v to φ/R obtained for binary and ternary films, we assumed the degree of agglomeration of $PC_{71}BM$ clusters has almost no change. The fitted value of $S_v/(\varphi/R)$ implied partially attached $PC_{71}BM$ clusters according to previous literature.[38] As a result, a more evenly distribution of P3HT semicrystallites in the ternary film which partitioned the intermixing domains into smaller regions would be the most reasonable explanation for the decrease of ξ. Together, we plotted the schematics of binary and ternary morphologies based on our fitting results, as shown in Fig. 4. Here the blue spheres represent $PC_{71}BM$ molecules and red blocks represent P3HT semicrystallites. In contrast to the binary film, ternary film has more evenly distributed P3HT semicrystallites, which will provide more continuous network for hole transport. Furthermore, more face-on oriented domains are known to be beneficial for vertical charge transport.[34,35] This morphology change could partially explain the observed reduced series resistance and increased FF in ternary cells. Moreover, the intermixing domains denoted in red dashed circles shrink drastically, which will shorten the charge transport pathways and greatly reduce the recombination rate within the intermixing domains. Consequently, more photocurrent generated in the intermixing region could be collected, contributing to the remarkable increase of J_{sc} in ternary cells. PTB7, the sensitizer, should have direct effect on the formation of new morphology. It disturbs the large scale P3HT crystallization forming a more evenly distributed structure. Instead of dispersing randomly in the film, PTB7 may wrap up the intermixing phase of P3HT/$PC_{71}BM$, hence limit its correlation length, or it may also wrap up the P3HT crystallites inducing face-on orientation. Furthermore, due to the cascade energy level, PTB7 chain is able to act as a charge transfer bridge when it is between or crossing different phases. To study the surface morphology of thin films, we also performed the atomic force microscope (AFM) measurements (Fig. S6†). Slightly larger surface roughness was observed for the ternary film, consistent with the ternary morphology with more evenly distributed domains.

Conclusion

In summary, we fabricated a series of P3HT : PTB7:$PC_{71}BM$ ternary solar cells with various mass ratios and film thicknesses. With the optimized mass ratio (P3HT : PTB7 : $PC_{71}BM$ = 16 : 1 : 17.5) and relatively thin film thickness (~100 nm), a 25% increase of PCE (from 4.0% to 5.0%) was achieved mainly due to the improvement in J_{sc} (from 11.1 mA cm^{-2} to 12.9 mA cm^{-2}) and FF (from 56% to 60%). Remarkably, ternary devices exhibited much less performance deterioration with the increase of the film thickness. Devices with optimized mass ratio outperformed not only the P3HT:$PC_{71}BM$ cells but also PTB7:$PC_{71}BM$ cells in a 200 nm thick film. GIWAXS/GISAXS measurements were carried out to search for the reason of device improvement due to the morphology differences between binary and ternary films since tiny improvement in photoabsorption was detected. The results implied that although the small amount of PTB7 barely contributed to the scattering intensity, it did change the morphology of the ternary films in terms of polymer packing and phase separation. It

Published on 13 October 2015. Downloaded by National Chiao Tung University on 13/11/2015 00:49:01.

slightly decreased the population of P3HT semicrystallite domains but at the same time produced more preferred face-on oriented domains. The length scale of the intermixing domain is almost halved in ternary film, which would significantly improve the charge collection from the intermixing region and lead to the enhanced photocurrent and PCE observed in our devices. Note here, the origin of the new morphology in ternary film is still unclear. The incorporation of PTB7 might change the formation energy of each phase and result in new arrangement within the film. Here, PTB7 must reside in the intermixing domain since no obvious length scale change in P3HT semicrystallite domains and $PC_{71}BM$ domains were observed. The existence of PTB7 in the intermixing domains could facilitate the charge separation and suppress the exciton recombination through the cascade energy alignment in addition to the photoabsorption contribution. It also could act as bridges to help the charges find the right pathway leading to the contact. Our study suggests a brand new route for high efficiency thick-film photovoltaic devices, which is to combine a high crystallinity polymer (*e.g.* P3HT) with a high efficiency polymer (*e.g.* PTB7). Based on this rule, it would be interesting to try new ternary systems that can incorporate more high efficiency polymer to further improve the photoabsorption in the future work.

Acknowledgements

We gratefully thank the beam time and technical supports provided by 23A SWAXS beamline at NSRRC, Hsinchu and BL14B1 and 16B1 beamlines at SSRF, Shanghai. We acknowledge the financial support from Research Grant Council of Hong Kong (General Research Fund No. 2130394, Theme-based Research Scheme No. T23-407/13-N and CUHK Direct Grant No. 4053128).

References

1 J. S. Moon, J. Jo and A. J. Heeger, *Adv. Energy Mater.*, 2012, **2**, 304–308.
2 Y. Liang, Z. Xu, J. Xia, S. T. Tsai, Y. Wu, G. Li, C. Ray and L. Yu, *Adv. Mater.*, 2010, **22**, E135–E138.
3 P. W. M. Blom, V. D. Mihailetchi, L. J. A. Koster and D. E. Markov, *Adv. Mater.*, 2007, **19**, 1551–1566.
4 L. C. Zeng, C. W. Tang and S. H. Chen, *Appl. Phys. Lett.*, 2010, **97**, 053305.
5 J. Peet, L. Wen, P. Byrne, S. Rodman, K. Forberich, Y. Shao, N. Drolet, R. Gaudiana, G. Dennler and D. Waller, *Appl. Phys. Lett.*, 2011, **98**, 043301.
6 W. Li, K. H. Hendriks, W. S. Roelofs, Y. Kim, M. M. Wienk and R. A. Janssen, *Adv. Mater.*, 2013, **25**, 3182–3186.
7 T. L. Nguyen, H. Choi, S. J. Ko, M. A. Uddin, B. Walker, S. Yum, J. E. Jeong, M. H. Yun, T. J. Shin, S. Hwang, J. Y. Kim and H. Y. Woo, *Energy Environ. Sci.*, 2014, **7**, 3040–3051.
8 A. Tayebeh, K. Parisa, M. Jie and J. B. Christoph, *Adv. Mater.*, 2013, **25**, 4245–4266.
9 L. Luyao, X. Tao, C. Wei, S. L. Erik and Y. Luping, *Nat. Photonics*, 2014, **8**, 716–722.
10 L. Bogyu, T. B. Jason, P. Andrew, D. M. Michael and S. Alan, *ACS Appl. Mater. Interfaces*, 2014, **6**, 6905–6913.
11 H. Satoshi, Y. Seiichirou, O. Hideo, B. Hiroaki and I. Shinzaburo, *J. Phys. Chem. C*, 2011, **115**, 11306–11317.
12 H. Jen-Hsien, V. Marappan, H. Kuo-Chuan, L. Jiann-Tsuen and C. Chih-Wei, *J. Mater. Chem.*, 2010, **20**, 2820.
13 C. Hyojung, C. Dae, B. Suk, L. Min-Jung, A. Tae, H. Jihun, K. Kyung, K. Yun-Hi, C. Dong and P. Chan, *Adv. Funct. Mater.*, 2013, **23**, 1556–1565.
14 W. Wenbin, Z. Fujun, L. Lingliang, Z. Miao, A. Qiaoshi, W. Jian and S. Qianqian, *J. Mater. Chem. C*, 2015, **3**, 7386–7393.
15 X. Lu, H. Hlaing, D. S. Germack, J. Peet, W. H. Jo, D. Andrienko, K. Kremer and B. M. Ocko, *Nat. Commun.*, 2012, **3**, 795.
16 Z. C. He, C. M. Zhong, S. J. Su, M. Xu, H. B. Wu and Y. Cao, *Nat. Photonics*, 2012, **6**, 591–595.
17 B. C. Thompson and J. M. Frechet, *Angew. Chem., Int. Ed.*, 2008, **47**, 58–77.
18 J. Dai, X. Jiang, H. Wang and D. Yan, *Appl. Phys. Lett.*, 2007, **91**, 253503.
19 T. Tominaga, K. Hayashi and N. Toshima, *Appl. Phys. Lett.*, 1997, **70**, 762.
20 Y. Huang, E. J. Kramer, A. J. Heeger and G. C. Bazan, *Chem. Rev.*, 2014, **114**, 7006–7043.
21 D. Wang, F. Liu, N. Yagihashi, M. Nakaya, S. Ferdous, X. Liang, A. Muramatsu, K. Nakajima and T. P. Russell, *Nano Lett.*, 2014, **14**, 5727–5732.
22 B. A. Collins, E. Gann, L. Guignard, X. He, C. R. McNeill and H. Ade, *J. Phys. Chem. Lett.*, 2010, **1**, 3160–3166.
23 F. Physical review lettersNano LettProceedings of the National Academy of SciencesMachuiS. Rathgeber, N. Li, T. Ameri and C. J. Brabec, *J. Mater. Chem.*, 2012, **22**, 15570–15577.
24 W. Chen, M. P. Nikiforov and S. B. Darling, *Energy Environ. Sci.*, 2012, **5**, 8045–8074.
25 U. S. Jeng, C. H. Su, C.-J. Su, K.-F. Liao, W.-T. Chuang, Y.-H. Lai, J.-W. Chang, Y.-J. Chen, Y.-S. Huang, M.-T. Lee, K.-L. Yu, J.-M. Lin, D.-G. Liu, C.-F. Chang, C.-Y. Liu, C.-H. Chang and K. S. Liang, *J. Appl. Crystallogr.*, 2009, **43**, 110–121.
26 P. Muller-Buschbaum, *Adv. Mater.*, 2014, **26**, 7692–7709.
27 X. Lu, H. Hlaing, D. S. Germack, J. Peet, W. H. Jo, D. Andrienko, K. Kremer and B. M. Ocko, *Nat. Commun.*, 2012, **3**, 795.
28 M. C. Chen, D. J. Liaw, Y. C. Huang, H. Y. Wu and Y. Tai, *Sol. Energy Mater. Sol. Cells*, 2011, **95**, 2621–2627.
29 H.-C. Liao, C.-S. Tsao, Y.-T. Shao, S.-Y. Chang, Y.-C. Huang, C.-M. Chuang, T.-H. Lin, C.-Y. Chen, C.-J. Su, U. S. Jeng, Y.-F. Chen and W.-F. Su, *Energy Environ. Sci.*, 2013, **6**, 1938.
30 W. R. Wu, U. S. Jeng, C. J. Su, K. H. Wei, M. S. Su, M. Y. Chiu, C. Y. Chen, W. B. Su, C. H. Su and A. C. Su, *ACS Nano*, 2011, **5**, 6233–6243.
31 N. D. Treat, C. G. Shuttle, M. F. Toney, C. J. Hawker and M. L. Chabinyc, *J. Mater. Chem.*, 2011, **21**, 15224–15231.
32 M. Shao, J. Keum, J. Chen, Y. He, W. Chen, J. F. Browning, J. Jakowski, B. G. Sumpter, I. N. Ivanov, Y. Z. Ma,

 This journal is © The Royal Society of Chemistry 2015

Published on 13 October 2015. Downloaded by National Chiao Tung University on 13/11/2015 00:49:01.

C. M. Rouleau, S. C. Smith, D. B. Geohegan, K. Hong and K. Xiao, *Nat. Commun.*, 2014, **5**, 3180.
33 A. L. Patterson, *Phys. Rev.*, 1939, **56**, 5.
34 H. Sirringhaus, P. J. Brown, R. H. Friend, M. M. Nielsen, K. Bechgaard, B. M. W. Langeveld-Voss, A. J. H. Spiering, R. A. J. Janssen, E. W. Meijer, P. Herwig and D. M. de Leeuw, *Nature*, 1999, **401**, 685–688.
35 J. R. Tumbleston, B. A. Collins, L. Yang, A. C. Stuart, E. Gann, W. Ma, W. You and H. Ade, *Nat. Photonics*, 2014, **8**, 385–391.
36 T. Xiao, H. Xu, G. Grancini, J. Mai, A. Petrozza, U. S. Jeng, Y. Wang, X. Xin, Y. Lu, N. S. Choon, H. Xiao, B. S. Ong, X. Lu and N. Zhao, *Sci. Rep.*, 2014, **4**, 5211.
37 S. J. Lou, J. M. Szarko, T. Xu, L. Yu, T. J. Marks and L. X. Chen, *J. Am. Chem. Soc.*, 2011, **133**, 20661–20663.
38 H. C. Liao, C. S. Tsao, T. H. Lin, C. M. Chuang, C. Y. Chen, U. S. Jeng, C. H. Su, Y. F. Chen and W. F. Su, *J. Am. Chem. Soc.*, 2011, **133**, 13064–13073.
39 M. Y. Chiu, U. S. Jeng, C. H. Su, K. S. Liang and K. H. Wei, *Adv. Mater.*, 2008, **20**, 2573–2578.
40 J. W. Kiel, A. P. Eberle and M. E. Mackay, *Phys. Rev. Lett.*, 2010, **105**, 168701.
41 N. D. Treat, M. A. Brady, G. Smith, M. F. Toney, E. J. Kramer, C. J. Hawker and M. L. Chabinyc, *Adv. Energy Mater.*, 2011, **1**, 82–89.
42 E. Y. Sheu, *Phys. Rev. A*, 1992, **45**, 2428–2438.
43 X. H. Lu, S. G. J. Mochrie, S. Narayanan, A. R. Sandy and M. Sprung, *Phys. Rev. Lett.*, 2008, **100**, 045701.
44 G. Nagele, *Phys. Rep.*, 1996, **272**, 216–372.
45 O. K. O. Glatter, *Small-Angle X-Ray Scattering*, Academic Press, London, 1982.
46 P. E. Shaw, A. Ruseckas and I. D. W. Samuel, *Adv. Mater.*, 2008, **20**, 3516–3520.

This journal is © The Royal Society of Chemistry 2015